Antiviral Research 86 (2010) 276–285

Contents lists available at ScienceDirect

Antiviral Research

journal homepage: www.elsevier.com/locate/antiviral

Compounds that target host cell proteins prevent varicella-zoster virus replication in culture, ex vivo, and in SCID-Hu mice

Jenny Rowe, Rebecca J. Greenblatt, Dongmei Liu, Jennifer F. Moffat*

Department of Microbiology and Immunology, State University of New York Upstate Medical University, 750 East Adams Street, Syracuse, NY 13210, USA

ARTICLE INFO

Article history:
Received 30 November 2009
Received in revised form 12 February 2010
Accepted 12 March 2010

Keywords:
Varicella-zoster virus
Antiviral
Cyclin dependent kinase
Roscovitine
Kinase inhibitor
Skin organ culture
SCID-Hu mouse

ABSTRACT

Varicella-zoster virus (VZV) replicates in quiescent T cells, neurons, and skin cells. In cultured fibroblasts (HFFs), VZV induces host cyclin expression and cyclin-dependent kinase (CDK) activity without causing cell cycle progression. CDK1/cyclin B1 phosphorylates the major viral transactivator, and the CDK inhibitor roscovitine prevents VZV mRNA transcription. We investigated the antiviral effects of additional compounds that target CDKs or other cell cycle enzymes in culture, ex vivo, and in vivo. Cytotoxicity and cell growth arrest doses were determined by Neutral Red assay. Antiviral effects were evaluated in HFFs by plaque assay, genome copy number, and bioluminescence. Positive controls were acyclovir (400 μM) and phosphonoacetic acid (PAA, 1 mM). Test compounds were roscovitine, aloisine A, and purvalanol A (CDK inhibitors), aphidicolin (inhibits human and herpesvirus DNA polymerase), L-mimosine (indirectly inhibits human DNA polymerase), and DRB (inhibits casein kinase 2). All had antiviral effects below the concentrations required for cell growth arrest. Compounds were tested in skin organ culture at EC_{99} doses; all prevented VZV replication in skin, except for aloisine A and purvalanol A. In SCID mice with skin xenografts, roscovitine (0.7 mg/kg/day) was as effective as PAA (36 mg/kg/day). The screening systems described here are useful models for evaluating novel antiviral drugs for VZV.

1. Introduction

Varicella-zoster virus (VZV) is the human-restricted alphaherpesvirus that causes varicella (chickenpox) upon primary infection and zoster (shingles) upon reactivation from latency. The incidence of zoster is highest in older people and those who are immunocompromised due to HIV/AIDS, malignancies, organ transplant, or high-dose corticosteroid therapy (Johnson et al., 2008). VZV reactivation may cause severe acute pain or neurological damage, and other complications include vision loss (zoster ophthalmicus) or chronic pain of indefinite duration (postherpetic neuralgia) (reviewed in Cohen and Straus, 2001). A live attenuated vaccine, Varivax (Merck & Co.), is available in the United States for pediatric varicella, but breakthrough cases occur, and it is not known what effect vaccination will have on geriatric zoster (Vázquez et al., 2004). Recently, the vaccine Zostavax (Merck & Co.) was approved in the U.S. for the prevention of zoster in adults older than 60 years (Holcomb and Weinberg, 2006). However, because many zoster patients are immunosuppressed and cannot be given a live vaccine or mount a strong response, there will continue to be a demand for antiviral drugs. Several chemotherapeutics for VZV infections are in use, but resistance can arise and treatment must begin within 72 h of onset for efficacy (Sampathkumar et al., 2009). The current drugs are nucleoside analogs that target virus DNA polymerase and may depend on virus thymidine kinase activity (De Clercq, 2004). There is a clear need for additional treatments for zoster because the populations at highest risk, the elderly and the immunocompromised, are increasing globally (Vafai and Berger, 2001).

An alternative paradigm for antiviral drug discovery is to target host cell functions that are required for virus replication. This has been a successful strategy in treating hepatitis C virus (HCV) infections with pegylated interferon (Zeuzem, 2008), and may be used in the future to block HIV genome synthesis by targeting cyclin dependent kinase 9 (CDK9) (Wang and Fischer, 2008). A number of studies have shown that cyclin dependent kinases (CDKs) are valid drug targets for herpesviruses. The CDK inhibitors roscovitine and purvalanol A prevent replication of human cytomegalovirus (Bresnahan et al., 1997; Sanchez et al., 2004), herpes simplex virus type 1 (Schang et al., 2000), Epstein-Barr virus (Knockaert et al., 2000; Kudoh et al., 2004), and VZV (Moffat et al., 2004; Taylor et al., 2004) in cultured cells. The antiviral mechanism of action of CDK inhibitors is not well understood for these herpesviruses, and has been revealed slowly. While investigating the antiviral mechanism of roscovitine for VZV, we found that (1) roscovitine treatment prevents virus mRNA transcription (Taylor et al., 2004); (2) VZV infection induces cyclin D3 and B1 expression and dysregulates

* Corresponding author. Tel.: +1 315 464 5454; fax: +1 315 464 4417.
E-mail addresses: rowej@upstate.edu (J. Rowe), rjgreenblatt@yahoo.com (R.J. Greenblatt), liud@upstate.edu (D. Liu), moffatj@upstate.edu (J.F. Moffat).

0166-3542/$ – see front matter © 2010 Elsevier B.V. All rights reserved.
doi:10.1016/j.antiviral.2010.03.007

CDKs in cultured human skin fibroblasts (Leisenfelder and Moffat, 2006); and (3) that cyclin B1/cdk1 complexes are localized in the cytoplasm of infected cells where the active enzyme is incorporated into newly assembled virions (Leisenfelder et al., 2008). This work also showed that cyclin B1/cdk1 phosphorylates the major immediate early transactivator, IE62, which is an essential VZV protein.

A panel of CDK inhibitors and anti-mitotic compounds was selected for this study based on their interactions with the cell cycle. L-Mimosine is an amino acid from plants that chelates iron and zinc and is commonly used in mammalian cell culture to synchronize cells at the G1/S phase border (Prather et al., 1999; Renò et al., 1999). The mechanism of action is not entirely defined, but L-mimosine was found to inhibit transcription of zinc-inducible genes involved in cell cycle progression, specifically the serine hydroxymethyltransferase gene, SHMT1, thus blocking DNA synthesis during S phase (Perry et al., 2005). The CK2 inhibitor DRB was selected because CK2 phosphorylates a plethora of proteins in DNA and RNA synthesis complexes and is involved in cell proliferation (Meggio et al., 1990; Meggio and Pinna, 2003; Pinna and Meggio, 1997). More importantly, many viral proteins are substrates of CK2, including VZV glycoprotein E and ORF63 and ORF65 proteins (Alconada et al., 1996; Cohen et al., 2001; Mueller et al., 2009; Yao et al., 1993). CDK1 is known to phosphorylate at least two important VZV proteins, glycoprotein I (Ye et al., 1999) and IE62 (Leisenfelder et al., 2008), thus CDK inhibitors purvalanol A and aloisine A were evaluated alongside roscovitine (racemic, R and S enantiomers), a similar compound that we showed prevents VZV replication in cultured cells (Taylor et al., 2004). Purvalanol A and aloisine A primarily inhibit CDK1 and cause cell cycle arrest at G1/S or G2, depending on the cell type (Corbel et al., 2009; Knockaert et al., 2002; Mettey et al., 2003; Villerbu et al., 2002). At higher concentrations, they have additional targets including other CDKs, GSK3α/β, ERK1/2, and pyridoxal kinase. Aphidicolin inhibits both viral and human DNA polymerase, causing cell cycle arrest in S phase, and has known antiviral activity for the alphaherpesviruses HSV-1 and PRV (Pedrali-Noy and Spadari, 1980; Verri et al., 1994). Acyclovir and phosphonoacetic acid were selected as positive control drugs because they have known mechanisms of antiviral activity (De Clercq, 2004; Huang et al., 1976; Reardon and Spector, 1989).

Directing drug therapies at the host may cause cytotoxicity and adverse events, although this problem may be less serious than expected if viruses are highly sensitive to inhibition of cell functions, or if they depend on cell functions that are induced by the virus. This latter effect was observed in cultured primary fibroblasts where the c-Jun N-terminal kinase (JNK) pathway was activated only in VZV-infected cells, and the JNK inhibitor SP600125 prevented VZV spread at low concentrations (Zapata et al., 2007). One advantage of targeting host cell functions for antiviral therapy is that resistance is unlikely to arise through mutations in the virus genome. Indeed, efforts to isolate a strain of VZV resistant to roscovitine failed after 10 weeks of continuous culture at doses below the EC_{50} (authors' observations). Many small molecules exist that inhibit host cell pathways, such as cell cycle and intracellular signaling, upon which viruses depend for replication and assembly. Some licensed drugs that are already approved for treating other diseases, especially cancer, may have unexplored antiviral properties.

Hypothesizing that roscovitine and additional cell cycle inhibitors would be effective against VZV, we tested a panel of compounds first in primary human fibroblasts (HFFs) and then in human skin organ culture (SOC). Lastly, we utilized SCID mice implanted with human skin xenografts and in vivo bioluminescence imaging to evaluate the antiviral effects of roscovitine and purvalanol A in animals. The general findings of this study were that anti-mitotic inhibitors prevented VZV replication in cultured cells, whereas aloisine A and purvalanol A lacked efficacy in skin organ culture. The results in SOC predicted the efficacy of roscovitine and the failure of purvalanol A in the SCID-Hu model.

2. Materials and methods

2.1. Propagation of cells and virus

MeWo cells, (a human melanoma cell line provided by Charles Grose, University of Iowa), and human foreskin fibroblasts (HFFs, CCD-1137Sk, American Type Culture Collection, Manassas, VA) were grown in Eagle's minimum essential medium with Earle's salts and L-glutamine (HyClone Laboratories, Logan, UT), supplemented with 10% heat-inactivated fetal bovine serum (Gemini Bio Products, West Sacramento, CA), penicillin–streptomycin (5000 IU/mL), amphotericin B (250 μg/mL), and nonessential amino acids (Mediatech, Herndon, VA). HFFs were subconfluent in all assays and were used prior to passage 20. VZV-BAC-Luc was derived from the parental Oka strain, a wild type clinical isolate from Japan (accession number: AB097933). A master stock of VZV-BAC-Luc (passage 10) was obtained from Dr. Hua Zhu (UMDNJ-New Jersey Medical School, Newark, NJ). VZV-BAC-Luc was stored at −80 °C and grown on HFFs for up to 10 passages. HFFs were infected with cell-associated VZV-BAC-Luc showing more than 80% cytopathic effect (CPE) at a 1:10 ratio of infected to uninfected cells and adsorbed for 2 h at 37 °C under 5% CO_2.

2.2. Preparation of drugs

All drugs were diluted to the stock solutions in dimethylsulfoxide (DMSO) unless otherwise indicated, aliquoted, and stored at −20 °C until use. The stock concentration, vendor and catalog number for each compound are listed: DMSO, Fisher, BP231-1; Acyclovir (ACV), 40 mM, Calbiochem, 114798; phosphonoacetic acid (PAA), 714 mM in culture medium, Sigma, 284270; L-mimosine, 20 mM in 20 mM NaOH, Sigma, M0253; dichloro-β-D-ribofuranosylbenzimidazole (DRB), 50 mM, Calbiochem, 287891; Aphidicolin, 20 mM, Sigma, A0781; Aloisine A, 20 mM, Calbiochem, 128125; Purvalanol A, 5 mM, Calbiochem, 540500, or Tocris, 1580; Roscovitine, 20 mM, Calbiochem, 557360; *R*- and *S*-Roscovitine, 20 mM, a kind gift from Dr. Laurent Meijer, C.N.R.S., Roscoff, France. Final drug dilutions were prepared fresh in complete tissue culture medium and warmed to 37 °C before use.

2.3. Cytotoxicity assays

The neutral red (NR) cytotoxicity assay was performed exactly as described in Zapata et al. (2007), which is based on the method of Babich et al. (2002). Each compound was tested in sets of 6 replicates at a range of concentrations from zero (diluent alone) to the upper limit of solubility. The treatments were refreshed every 24 h. The amount of diluent for every dose was equivalent to that at the highest dose. A positive control for cell death was staurosporine (35 nM), which is a broad-spectrum kinase inhibitor that causes apoptosis (Kabir et al., 2002).

The recovery of VZV titer after drug treatment was a second assay for cytotoxicity. HFFs were inoculated with VZV at MOI = 0.01 and treated with either: (1) diluent for 48 h, (2) compound for 48 h, or (3) compound for 24 h followed by diluent for 24 h. Compound was refreshed daily. Duplicate samples were harvested by trypsinization at time 0, 24, and 48 h and the cell suspensions were titered on separate MeWo cell monolayers as described in Moffat et al. (1998).

2.4. Antiviral plaque assay and quantitative PCR

The effects of drug concentration on VZV replication were tested as in (Zapata et al., 2007) for 48 h. Virus yield was determined by infectious focus assay (Moffat et al., 1998) or quantitative PCR (Taylor et al., 2004). For qPCR, the oligonucleotide primers and probe for human β-globin were 5′-CCTGATGCTGTTATGGGCAA-3′ (forward), 5′-CCAGGCCATCACTAAAGGCA-3′ (reverse), and FAM-5′-CTAAGGTGAAGGCTCATGGCAAGAAAGTGCT-3′-TAMRA (probe).

2.5. Skin organ culture

Human fetal skin tissue, 13–24 weeks gestational age, was obtained in accordance with all local, state, and federal guidelines from Advanced Bioscience Resources (Alameda, CA). Cultivation and inoculation of the tissue by scarification with VZV-BAC-Luc was performed as in Taylor and Moffat (2005). Briefly, skin was cut into pieces approximately 1-cm^2, maintained in culture on NetWells above 1.0 mL tissue culture medium, and then inoculated with VZV-BAC-Luc. The dermal side of the VZV-infected skin tissue was in contact with the culture medium that contained the test compound or diluent. Virus replication was measured by bioluminescence imaging (see below).

2.6. Animal procedures

Human fetal skin xenografts were introduced subcutaneously into 7–8-week-old NOD.Cg-Prkdc Il2Rγ^{null} SCID mice (Jackson Laboratories, Bar Harbor, ME) as full-thickness dermal grafts as described previously with the exception that single implants were used instead of bilateral implants (Moffat et al., 1995). At 4–5 weeks after implantation, implants were inoculated with cell-associated VZV-BAC-Luc in HFFs, and viral growth was monitored using bioluminescence imaging. Implants were inoculated by scarification by: (1) placing 30 μL of infected cell suspension onto the surface of the implant using a volumetric stepper, (2) scratching five times in one direction and five times at 90° angles with a 27-gauge needle, and (3) placing an additional 30 μL of virus onto the abraded surface of the skin. PAA and roscovitine were administered by implanting Alzet osmotic pumps (DURECT Corporation, Cupertino, CA) subcutaneously over the right flank of the mouse. Alzet osmotic pumps, model 2001, administer 1.0 μL of drug per hour over the course of 7 days. Purvalanol A was administered via daily i.p. injection. Mice were weighed prior to treatment on imaging Day 1 and again upon termination of the experiment. The average body weight difference (ABWD) was calculated for each test group by subtracting the average final weight from the average initial weight. Mice were euthanized and implants harvested after treatment had ended. The protocol was reviewed and approved by the Committee for Humane Use of Animals at SUNY Upstate Medical University.

2.7. Bioluminescence imaging

Imaging was performed with a cooled CCD camera (Xenogen IVIS-50 or −200 series, Caliper Life Sciences, Hopkinton, MA). Pseudocolored images of photon emissions were overlaid on grayscale images of the whole tissue culture plate or mouse in order to assist with spatial localization of the luciferase signals. In culture: Tissue culture medium was removed daily from wells and replaced with 1.0 mL D-luciferin (300 μg/mL in PBS) and incubated for 1 h at 37 °C. Each plate was imaged using the IVIS-50 for 1 min. Standard regions of interest (ROIs) were drawn around each of the wells in the plate and total flux (photons/s) values were obtained using Living Image 3.1 software. Ex vivo: Skin was removed from the NetWells daily and transferred to black 24-well plates. D-Luciferin solution was added for 1 h and each plate was imaged for 1 min using the IVIS-50. D-Luciferin substrate was removed after imaging and replaced with fresh drug-containing medium every 24 h. ROIs were free-drawn around each piece of skin and analyzed as above. In vivo: Mice were placed in an induction chamber and anesthetized with isoflurane (2% in oxygen). D-Luciferin (100 mg/kg i.p.) was administered and permeated the mouse for 10 min. Up to five mice at a time were placed into the IVIS-200 imaging chamber, where individual nosecones delivered continuous anesthesia. Images were acquired for an initial exposure time of 5 min; if pixels were saturated, additional images with shorter exposure times were acquired. Images were set to a minimum below background (3×10^3 photons/s) and ROIs were drawn over the implant and analyzed as above. Background for each mouse was determined by placing a 1-cm^2 ROI over the head; background for the entire cohort of mice averaged approximately 1×10^4 photons/s.

2.8. Data analysis and statistics

Bioluminescence data were obtained as total flux (photons/s). Total flux values from three replicate samples of VZV grown in HFFs or SOC at day 2 post infection were averaged, and the drug-treated group was compared to the diluent-treated group to determine the percent of total flux. The rate of VZV spread in skin xenografts in vivo was calculated as the slope of a line with $y = \log_{10}$(photons/s), and x = day of treatment, ranging from day 2 to 7. Virus growth rates were calculated for each mouse, and the average and standard deviation for each group were compared by the nonparametric Mann–Whitney U-test using GraphPad Prism 5.02 (GraphPad Software, San Diego, CA, www.graphpad.com). Error bars represent standard deviations; asterisks denote significance; $^*p \leq 0.05$; $^{**}p < 0.01$; $^{***}p < 0.001$.

3. Results

3.1. Cytotoxicity assays

When evaluating compounds for antiviral effects, it is critical to use concentrations that are not overtly cytotoxic, since any impairment to cell functions would affect virus replication. The cells used in this study were low-passage HFFs, a primary human skin cell type that is permissive for VZV both in vitro and in vivo. The potential cytotoxic effects of the selected compounds on HFFs were unknown, so neutral red (NR) dye uptake assays were performed. The NR dye is taken up by pinocytosis; the amount absorbed is directly proportional to cell number and membrane integrity (Repetto et al., 2008). The values from six replicates were obtained before treatment (time zero) and after 48 h, and then the averages were calculated. To determine whether the drugs inhibited cell growth or caused cell death, the fold change was calculated by dividing the average absorbance at 48 h by the average at time zero (Fig. 1). No live cells were detected after treatment with staurosporine, whereas DMSO had no effect up to 150 mM and inhibited cell growth slightly at 400 mM. This concentration of DMSO was at least eight times greater than used with the highest concentration of any drug. If the fold change was less than 1, the treatment was considered cytotoxic. Cytotoxic doses varied, with some compounds killing cells at micromolar concentrations (purvalanol A), while others (acyclovir, aphidicolin, aloisine A) were tolerated up through the limit of their solubility in culture medium at 37 °C (Table 1). All forms of roscovitine had a similar effect on HFFs, with cytotoxicity observed at 40 μM and higher. The data were also used to determine the concentration that blocked the growth of HFFs, defined as the lowest dose for which absorbance at 48 h was the same as absorbance at 0 h. The cell growth arrest dose was used to set the maximum concentration of each compound in subsequent antiviral assays in HFFs. For roscovitine and aloisine A, the maxi-

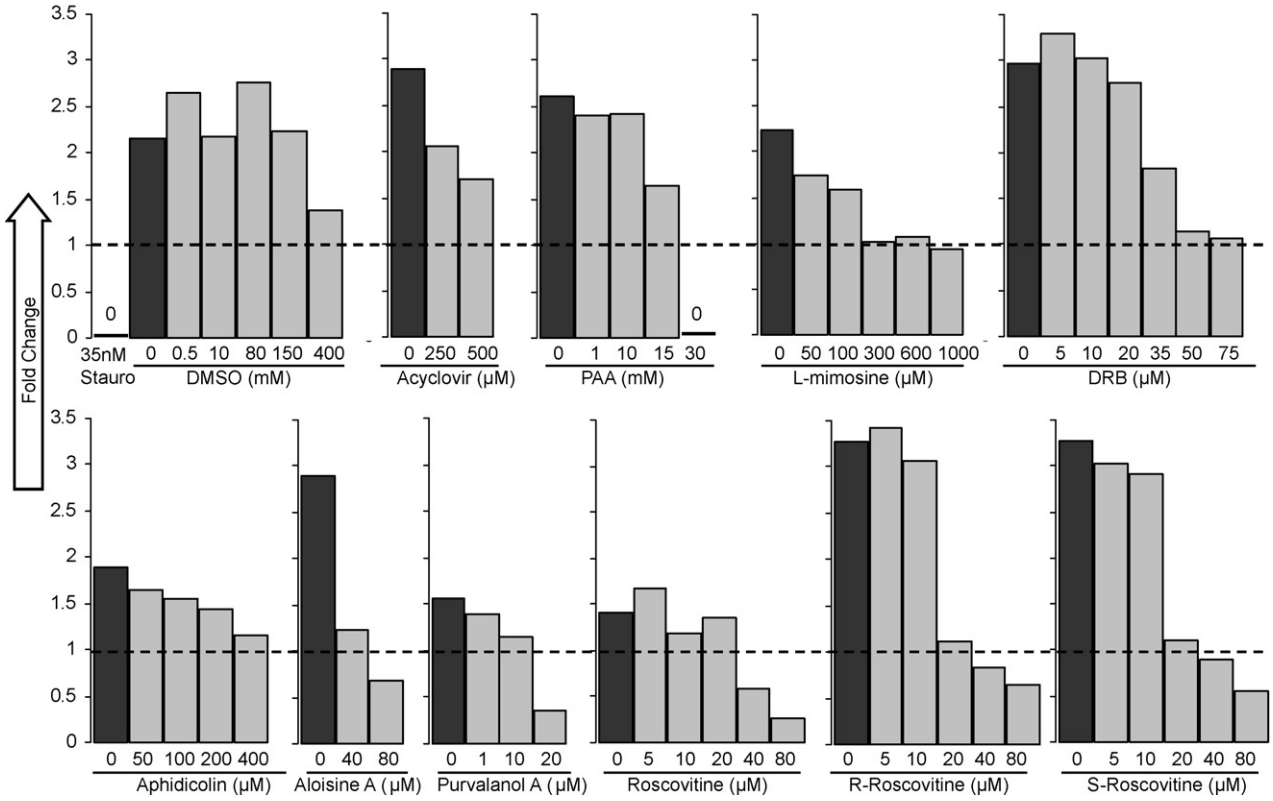

Fig. 1. Neutral red cytotoxicity assays. Subconfluent HFFs were treated in sets of six replicates for 48 h with compounds at the indicated concentrations. The concentration of diluent in each dose was equalized to the amount at the highest dose. Staurosporine (35 nM) was used to induce apoptosis and served as a positive control for cell death. Average absorbance (540 nm) of each group at 48 h was divided by the average absorbance at time zero and recorded as fold change. The dashed line indicates fold change equal to 1, which corresponds to no change in cell number. A fold change less than 1 indicates cytotoxicity. Cytotoxic and cell growth arrest doses are listed in Table 1.

mum concentration was set at 20 μM, and for purvalanol A it was 10 μM.

To further demonstrate that the inhibitors were not cytotoxic and to assess whether their antiviral effects were reversible, recovery assays of VZV yield were performed. Roscovitine was not evaluated because it was reversible in a previous study (Taylor et al., 2004). Infected HFFs were treated for 24 h at antiviral concentrations (as described below), and then the compound was removed for 24 h. If VZV titer recovered after the treatment phase, then the antiviral effects were considered reversible and the treatment non-cytotoxic. For all the compounds tested, VZV yield increased after the withdrawal of the compound (data not shown).

3.2. Antiviral assays

The effects of each compound on VZV replication were evaluated by two methods, infectious focus assay and real-time quantitative PCR. Each compound was tested in duplicate using a range of concentrations from zero (diluent alone) to the cell growth arrest dose. HFFs were inoculated with VZV at a low MOI (approximately 0.01) for 2 h, excess inoculum was removed and medium containing the compound was added; this point was deemed the start of the assay (time zero). Instead of proceeding with a typical plaque reduction assay that measures pfu in the original HFF culture, the infected and treated HFFs were harvested by trypsinization and titered on sep-

Table 1
Antiviral effects of cell cycle inhibitors against VZV.

Compound	Cytotoxic dose (μM)	Cell growth arrest dose	VZV EC_{50} (qPCR)	VZV EC_{50} (titer)	Selective index	Primary target(s)
DMSO	$>4.0 \times 10^5$	–	–	7.5×10^4	5	–
Acyclovir	$1.0 \times 10^{3*}$	–	5	4	250	Herpesvirus DNA pol
PAA	1.5×10^4	–	500	300	60	Herpesvirus DNA pol
L-mimosine	3.0×10^3	300	50	70	43	Serine hydroxyl-methyltransferases, DNA synthesis
DRB	>75	50	2	5	15	CK2
Aphidicolin	500*	80	0.5	0.6	833	Human DNA pol Herpesvirus DNA pol
Aloisine A	30*	20	2	2.5	12	CDK1, -2, -5, GSK-3alpha/beta
Purvalanol A	20	10	0.025	0.035	570	CDK1, -2, -5, -7, -9
Roscovitine (racemic)	40	20	2.5	4	10	CDK1, -2, -5, -7, -9
R-Roscovitine	40	20	3	3.5	11	CDK1, -2, -5, -7, -9
S-Roscovitine	40	20	1	2.5	16	CDK1, -2, -5, -7, -9

Compounds with selective indices of 10 or above are deemed antiviral. Negative control: DMSO. Positive controls: VZV polymerase inhibitors PAA and acyclovir. Abbreviations: DMSO: dimethyl sulfoxide; PAA: phosphonoacetic acid; DRB: dichloro-β-D-ribofurano-sylbenzimidazole. Symbols: (*) solubility limit; (–) not applicable and/or not determined.

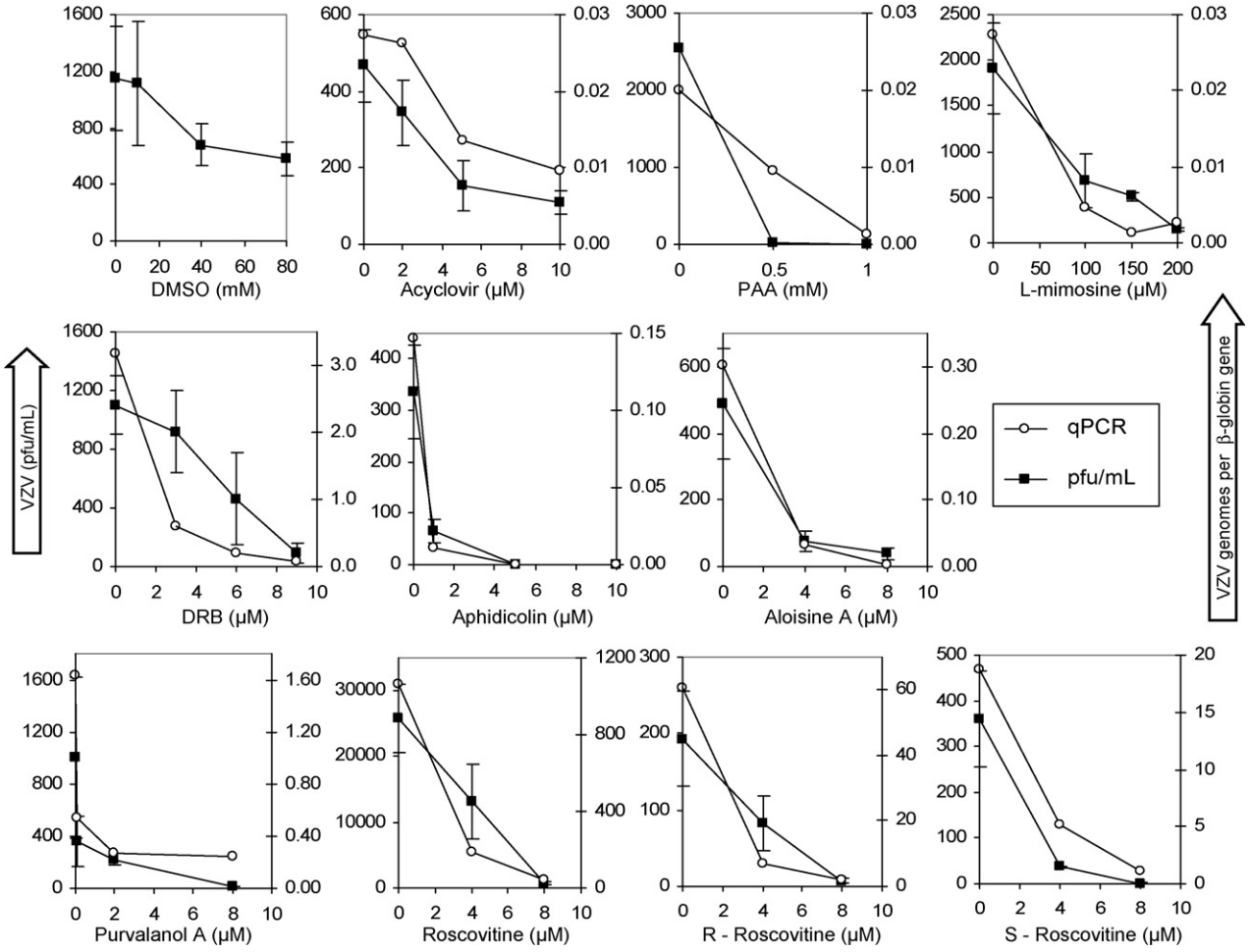

Fig. 2. Effects of drug treatment on VZV yield by infectious focus assay and qPCR. Subconfluent HFFs were treated with the compounds in duplicate for 48 h. Virus yield was determined by infectious focus assay and plaque-forming units (pfu)/mL were calculated (left axis, points are average ± standard deviation). The number of virus genomes was determined in quadruplicate by real-time TaqMan quantitative PCR (qPCR) and compared to the β-globin gene copy number (right axis).

arate MeWo cell monolayers. This approach measures VZV spread from the initial infected cell to neighboring cells and is the standard method for evaluating VZV replication. VZV growth was measured in this manner at 0, 24, 48, and 72 hpi, and DNA was isolated from an aliquot of the infected cell suspension for real-time quantitative PCR. QPCR for VZV ORF38 was performed in quadruplicate, as in (Taylor et al., 2004). ORF38 copy number was normalized to human β-globin copy number. The pfu/mL and VZV genome copies/β-globin copy were calculated and plotted against dose (Fig. 2). The EC_{50}s were interpolated from these results as the dose that caused a 50% reduction in VZV titer or normalized genome copy number. The two assay methods correlated well; EC_{50}s calculated by qPCR were within 2.6-fold of those calculated by infectious focus assay (Table 1). As expected, the established antiviral compounds acyclovir and PAA were highly effective. All other compounds had antiviral activity at concentrations that were substantially lower than the cell growth arrest doses. For example, 4- to 6-fold less L-mimosine was required to prevent VZV growth than HFF proliferation (Fig. 2, Table 1). The difference in the doses was more than 2 orders of magnitude for purvalanol A, with an EC_{50} of 35 nM and cell growth arrest observed above 10 μM. The CDK inhibitors roscovitine and aloisine A, which are chemically related to each other, had similar toxicity and efficacy profiles with EC_{50} values between 2 and 4 μM. Selective indices (SI), defined as the cytotoxic dose divided by the EC_{50} (obtained by plaque assay), were calculated for each compound and were all equal to or greater than 10. Aphidicolin and purvalanol A had particularly high SIs, which were 833 and 570, respectively.

3.3. Validation of VZV-BAC-Luc in culture

The strain of VZV used in this study, recombinant pOka (Niizuma et al., 2003), was cloned as a bacterial artificial chromosome with EGFP and firefly luciferase genes inserted in non-coding regions (Zhang et al., 2007). The construction of VZV-BAC-Luc enabled bioluminescence imaging to measure virus spread. To verify the benefit of this in vivo imaging system (IVIS) as an alternative method for measuring VZV yield in cultured cells, HFFs were inoculated with VZV and then imaged daily from 0–5 dpi by IVIS. Each day after imaging, one well was harvested for titration in an infectious focus assay. VZV-BAC-Luc growth kinetics were similar by IVIS and the infectious focus assay, demonstrating that bioluminescence was proportional to VZV yield (Fig. 3A); the correlation coefficient between the two assays was 0.92. To confirm the efficacy of the compounds against VZV-BAC-Luc, EC_{99} doses were tested and virus replication was measured by IVIS. HFFs were infected with cell-associated VZV-BAC-Luc and the culture plates were imaged daily using the IVIS-50 from 0 to 5 dpi. The reduction in bioluminescence from VZV-BAC-Luc at 2 dpi was 90% or greater for each compound, which was similar to results obtained with rPOka (Fig. 3B). VZV-BAC-Luc and IVIS were used for subsequent experiments using human skin tissues in organ culture and in mice. Bioluminescence

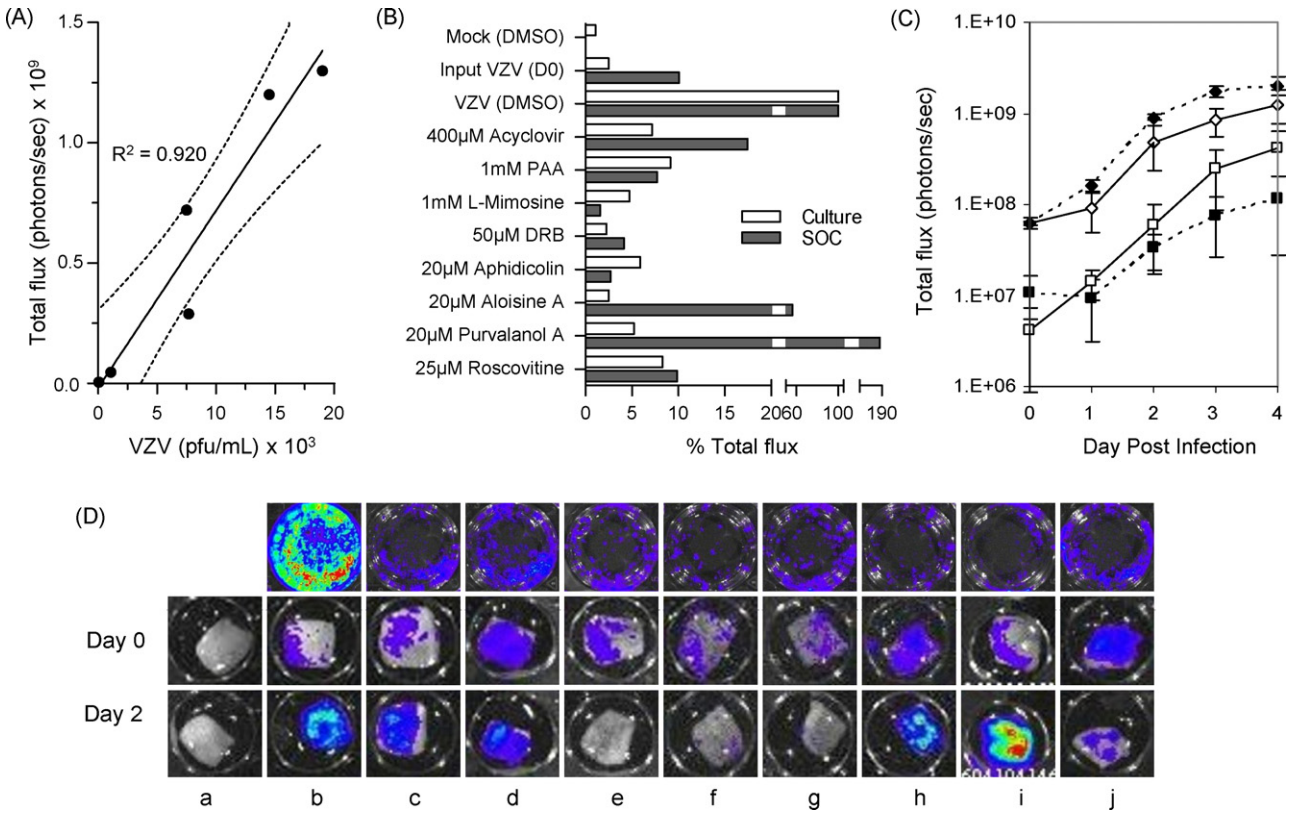

Fig. 3. (A) Comparison of VZV-BAC-Luc growth curves by IVIS and infectious focus assay. HFFs were infected with VZV-BAC-Luc and bioluminescence signal was measured daily in 6-well plates by IVIS (total flux = photons/s). Each day cells from duplicate wells were collected and then titered by infectious focus assay (pfu/mL). Results were graphed as VZV (pfu/mL) × 10^3 on the *x*-axis and total flux (photons/sec) × 10^9 on the *y*-axis. A line of best fit was plotted (solid line) with ±95% confidence intervals (dashed lines). $R^2 = 0.920$, indicating that 92% of the variance is shared between IVIS and infectious focus assay. Data obtained from the average of 2 wells. (B) Antiviral effects in culture and ex vivo measured by IVIS. HFFs or SOC infected with VZV-BAC-Luc were treated with the inhibitor panel. Bioluminescent images were taken daily using the IVIS and total flux was measured. Percent of total flux was calculated from the average of three wells or three pieces of skin per drug at 2 dpi: average total flux of drug was divided by the average total flux of VZV (DMSO) and multiplied by 100. All drugs tested exhibited antiviral activity. Mock samples were uninfected wells or DMSO treated skin. Input VZV was inoculum at Day 0. (C) Aloisine A and purvalanol A did not inhibit VZV replication in SOC. Growth curves in the SOC model were generated plotting total flux over 5 days. The trend of the resulting curves was typical of VZV growth (treated samples, dashed lines; controls, solid lines). Neither aloisine A (black squares) nor purvalanol A (black diamonds) reduced bioluminescent signals compared to the DMSO-treated controls (aloisine A control, open diamonds; purvalanol A control, open squares). (D) Representative bioluminescence images of HFFs and SOC. HFFs (top row) were infected with VZV-BAC-Luc and treated with DMSO (b) or the inhibitor panel (c–j) for 2 days. High total flux values (yellow and red) were observed in the control, indicating VZV growth, and low total flux values (blue and purple) were observed in all treated samples, indicating antiviral efficacy in culture. Skin (lower rows) was mock inoculated (a) or inoculated with VZV-BAC-Luc (b–j) and total flux was approximately equal in all samples on Day 0. By 2 dpi (bottom row), total flux increased in skin treated with DMSO (b), aloisine A (h), and purvalanol A (i), and decreased in all others. Treatments: DMSO (a, b), 400 μM acyclovir (c), 1 mM PAA (d), 1 mM L-mimosine (e), 50 μM DRB (f), 20 μM aphidicolin (g), 20 μM aloisine A (h), 20 μM purvalanol A (i), or 25 μM roscovitine (j). Images acquired using the IVIS-50 instrument. (For interpretation of the references to color in this figure legend, the reader is referred to the web version of the article.)

is preferable to infectious focus assay for measuring VZV replication in full-thickness skin because the tissue is difficult to disperse into a single-cell suspension, and other methods to disrupt tissue (sonication, freeze-thaw, enzymes) destroy VZV infectivity.

3.4. Antiviral activity in skin organ culture

Having established that the panel of compounds had antiviral effects in cultured HFFs, we then proceeded to evaluate them in skin where VZV infects epidermal keratinocytes as well as dermal fibroblasts. We hypothesized that the differentiated cell types and the tissue microenvironment in full-thickness human fetal skin would provide relevant conditions for evaluating compounds that target host cell functions. Using a SOC model we previously developed (Taylor and Moffat, 2005), the reporter virus VZV-BAC-Luc, and bioluminescence detection, it was possible to measure VZV replication repeatedly in the same tissue explants over several days. This enabled growth kinetics to be calculated accurately from limited amounts of skin tissue. Tissues were treated in triplicate with each compound at EC_{99} doses, or with diluent, and it was refreshed each day. Skin was imaged from 0 to 6 dpi using the IVIS-50. Previous studies showed that, when treated with DMSO alone, VZV replication in SOC reached a maximum by 4–5 dpi. Histopathological analysis of skin tissue showed that neither DMSO nor roscovitine was cytotoxic, and the integrity of the skin tissue was normal for up to 11 days in culture (Taylor and Moffat, 2005). Background signals were determined from mock-infected skin treated with DMSO diluent. Virus growth after 2 dpi was calculated by dividing the average total flux of the diluent-treated samples with the average total flux of the treated samples (Fig. 3B). The results in SOC were similar to the antiviral effects seen in cultured HFFs, using the same experimental conditions, for 1 mM PAA, 1 mM L-mimosine, 50 μM DRB, 20 μM aphidicolin, and 25 μM roscovitine. None of the compounds caused gross changes in the appearance of the skin tissue. In contrast, the antiviral effects of 400 μM acyclovir, 20 μM aloisine A, and 20 μM purvalanol A were much lower in SOC than in HFFs. The lack of antiviral activity displayed by 20 μM purvalanol A and 20 μM aloisine A in SOC was unexpected and reproducible over 5 days of virus infection (Fig. 3C). The differences in antiviral effects of the compounds were visible by 2 dpi in HFFs and SOC (Fig. 3D). All skin explants received an equivalent inoculum on day 0, and total flux increased in the explants treated with diluent. Acyclovir and PAA prevented VZV spread and total flux remained constant. L-Mimosine, DRB, aphidicolin and roscovitine reduced the total flux,

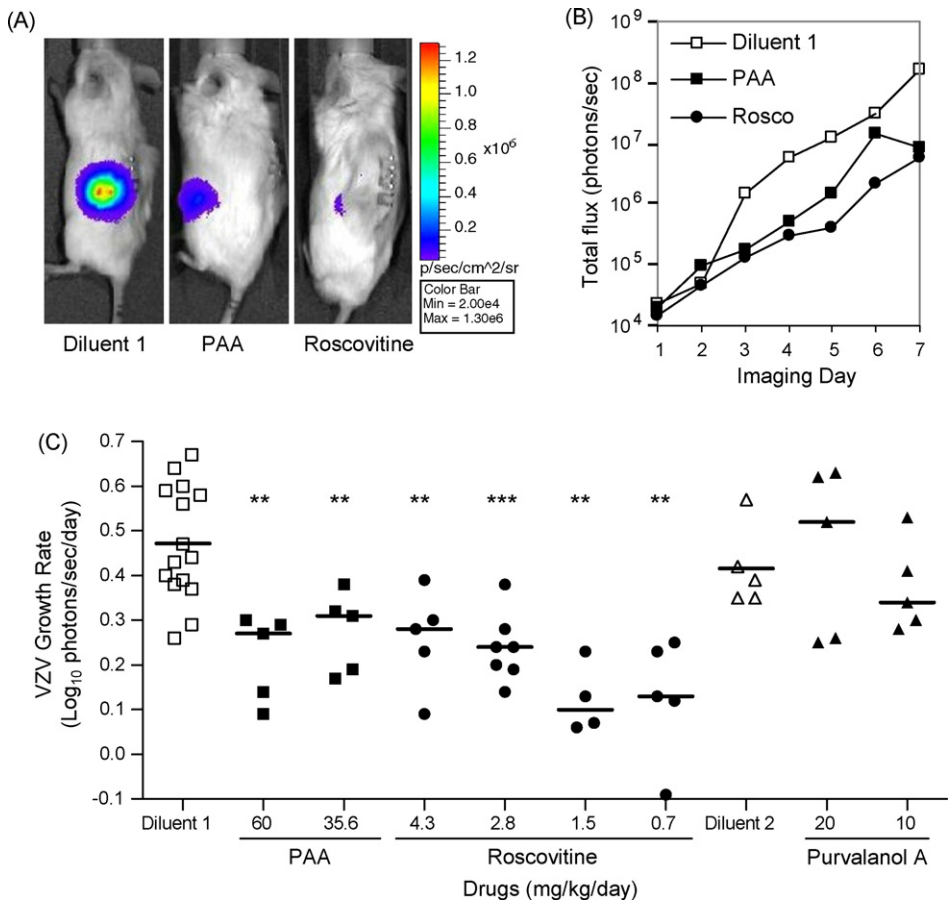

Fig. 4. (A) Representative bioluminescence images of SCID-Hu mice infected with VZV-BAC-Luc. A representative mouse from each of the three groups [diluent 1 (50% DMSO), PAA, and roscovitine] is shown at imaging Day 5, which corresponds to treatment Day 3. Bioluminescence signals were located on the left flank directly above the skin implant. Signal intensity was visibly reduced in both drug-treated mice compared to the diluent. Images were acquired with the IVIS-200 instrument; a pseudocolored image of photon emissions was overlaid on a grayscale photographic image of the mice. Scale: minimum = 2×10^4 total flux, maximum = 1.3×10^6 total flux. (B) Representative IVIS-200 results. Total flux was determined by drawing a ROI over the skin implant of the three mice shown in (A) and then plotted versus the imaging day. Although the bioluminescence signal for each of these mice began at approximately the same value, $\sim 2 \times 10^4$ total flux, the virus growth rate was slower in mice treated with PAA and roscovitine compared to the diluent. (C) PAA and roscovitine reduced VZV growth rate in vivo. The VZV growth rate was calculated for each mouse as $\log_{10}$ photons/s/day and plotted by treatment group (individual symbols). The average growth rate was calculated for each group (solid lines). Combining diluent-treated mice from all experiments ($n = 20$) produced an average growth rate of 0.46 ± 0.12, which is typical of VZV in cultured cells. A range of doses of PAA ($n = 10$ combined) and roscovitine ($n = 21$ combined) significantly reduced VZV growth rates. Purvalanol A ($n = 10$ combined) was not effective at reducing the rate of VZV growth. For details see Table 2. Data from three separate experiments are shown. Mann–Whitney *U*-two-tailed test: $^{**}p < 0.01$, $^{***}p < 0.001$. Diluent 1, 50% DMSO; Diluent 2, 50% DMSO and 25% EtOH in PBS.

whereas it increased in explants treated with aloisine A and purvalanol A. PAA and roscovitine were selected for further tests in vivo based on their efficacy in SOC. Purvalanol A was also selected to address whether its failure in SOC was predictive of efficacy in the SCID-Hu mouse model of VZV replication.

3.5. Roscovitine, but not purvalanol A, prevents VZV replication in vivo

Although the ex vivo skin organ culture system is a useful model, it only partially mimics the in vivo environment. It is conceivable that the failure of purvalanol A in skin explants, for example, was an artifact of the SOC model. To rule out this possibility, both purvalanol A and roscovitine were evaluated in the SCID-Hu mouse with skin implants. Skin was inoculated with VZV-BAC-Luc on Day 0 by scarification. Bioluminescence imaging began on Day 2 after excess inoculum had dispersed. To ensure that only mice with successfully infected implants were included in the experiment, assignment to treatment groups did not occur until the total flux had exceeded twice the background level ($\sim 2 \times 10^4$ photons/s). Thus, VZV infection was established prior to treatment, which reflects how patients with zoster are treated. Mice were randomly assigned to either treatment or control groups ($n = 4$–7). Treatment was for 7 days with either diluent (50% DMSO), PAA (60 or 35.6 mg/kg/day), or roscovitine (4.3, 2.8, 1.5, or 0.7 mg/kg/day) by placing subcutaneous osmotic pumps over the right flank. Purvalanol A (20 or 10 mg/kg/day) was administered by i.p. injection because the diluent was incompatible with the pump. Mice were imaged daily using the IVIS-200 over the course of treatment and continued for 1 day after it was stopped. Representative images of mice at imaging Day 5, which corresponds treatment Day 4 for the diluent and Day 3 for the test drugs, display the difference in total flux between treatment groups (Fig. 4A). Implants were visible on the left flank and the osmotic pump on the right. Total flux values were determined by drawing a ROI over the skin implant. These values were then plotted as the total flux (photons/s) versus the imaging day (Fig. 4B). The trend of the resulting curve for the diluent-treated mouse was typical of VZV growth.

In order to compare cohorts of mice, the rate of VZV spread in the skin implants was calculated from the day after treatment was initiated to the day after it ended ($y = \log_{10}$ photons/s/day, and $x =$ day of treatment). The average VZV growth rate was calculated for each group and expressed as the mean ± standard deviation (Fig. 4C, Table 2). Combined data from three separate experiments demon-

Table 2
Summary of in vivo SCID-Hu data.

Compound	Dose (mg/kg/day)	ABWD[a]	Mortality	Average VZV growth rate[b]	±SD[c]	Significance (p)[c]
Diluent 1[g]	–	−0.84	0/15	0.47	0.13	–
PAA	60.0[d]	0.14	0/5	0.22	0.10	0.005
PAA	35.6[e]	−4.40	0/5	0.27	0.09	0.010
Roscovitine	4.3[d]	0.36	0/5	0.26	0.11	0.010
Roscovitine	2.8[e]	−1.60	0/7	0.24	0.08	0.001
Roscovitine	1.5[e]	−0.10	0/4	0.12	0.08	0.003
Roscovitine	0.7[e]	−1.20	0/5	0.13	0.14	0.001
Diluent 2[g]	–	−1.45	2/6	0.42	0.09	–
Purvalanol A	20[f]	−2.96	4/6	0.45	0.19	0.834
Purvalanol A	10[f]	−0.99	1/6	0.37	0.10	0.295

[a] Average body weight difference (average final weight − average initial weight in grams).
[b] VZV growth rate ($\log_{10}$ photons/s/day).
[c] ±SD and p values determined using the Mann–Whitney U-two-tailed test.
[d] Drug doses determined based on average weight of mice per compound on Day 2 post infection.
[e] Drug doses determined based on average weight of mice per compound before infection.
[f] Drug doses determined based on average weight of mice per cage on Day 1 post infection.
[g] Diluent 1: 50% DMSO; Diluent 2: 50% DMSO, 25% EtOH in PBS.

strate that the average VZV growth rate in the mice treated with diluent was approximately double the growth rates in the PAA and roscovitine treatment groups. These results were significant using the Mann–Whitney U-two-tailed test (summarized in Table 2). Although several concentrations of roscovitine were tested in vivo, there were no significant differences between any of the roscovitine groups by the Mann–Whitney U-two-tailed test ($p \geq 0.05$).

None of the mice in these experiments showed signs of distress, either from VZV infection, surgery, drug treatments, or daily imaging procedures. The average body weight difference (ABWD) was determined for each test group within each experiment (Table 2). No difference was seen in the VZV growth rate of mice treated with purvalanol A at either dose, confirming the results obtained with the SOC model. Purvalanol A treatment and its diluent were not as well tolerated as roscovitine, and mortality increased without obvious weight loss.

4. Discussion

This study shows that a variety of CDK inhibitors and compounds that target host cell enzymes suppressed the growth of VZV in primary human cells, and that a subset were also effective in SOC and the SCID-Hu mouse models. The antiviral effects were observed at concentrations that did not cause cell cycle arrest in HFFs, suggesting that the mechanism of action was linked to the role of the enzyme target in VZV replication and not to cell division. The antiviral EC_{50} values were at least 5-fold less than the cell-cycle arrest doses; VZV is more sensitive to CDK inhibition than the cell cycle is in HFFs. CDK1 and CDK2 are the shared primary targets of aloisine A, purvalanol A and roscovitine (Meijer and Raymond, 2003), so it was surprising to find that only roscovitine had antiviral activity in SOC and SCID-Hu mice. This reinforces the importance of using models that employ fully differentiated, intact human tissues and live animals to evaluate antiviral activity. The SOC and SCID-Hu mouse models of VZV replication, combined with in vivo imaging of bioluminescent virus, together form a novel system that proved invaluable for screening unconventional antiviral compounds.

Bioluminescence imaging has emerged as a powerful approach for studying disease and therapeutics in mice (Dothager et al., 2009). In cancer research, bioluminescence imaging has commonly been used to measure the size and location of injected tumors that express luciferase, and then to monitor tumor regression in the same animal over time during treatment with anti-tumor agents. In virology research, the virus usually expresses luciferase and the site and extent of infection are detected by bioluminescence. This technique was very successful for studying the pathogenesis of HSV-1 and the antiviral effects of valacyclovir (Luker et al., 2002). Unlike HSV-1, which causes a systemic infection in mice, VZV is restricted to human tissue and only infects and replicates in human tissue xenografts in SCID mice. The number of SCID-Hu mice available for experimentation is limited by the amount of human tissue that can be obtained, the expertise required to surgically implant the tissue, and the need to house mice in isolator caging. A technique such as bioluminescence imaging is especially valuable because VZV infection can be monitored serially in the same animal. In addition to this study, one other group (Oliver et al., 2008; Wang et al., 2003) has used this approach, and they reported important aspects of VZV pathogenesis and marginal effectiveness of valacyclovir in SCID-Hu mice with skin xenografts. Adoption of in vivo imaging for VZV research was made possible only after the virus genome was cloned as a bacterial artificial chromosome, which was accomplished by several groups (Nagaike et al., 2004; Tischer et al., 2007; Yoshii et al., 2007; Zhang et al., 2007), and genes for luciferases were inserted. Bioluminescent strains of VZV offer a distinct advantage for accurate quantification of virus yield that is critical for evaluation of antiviral agents. Standard plaque assays for VZV often underestimate the amount of virus since it is highly cell-associated in cultured cells: most extracellular virions are defective, infectious virions are not released into the medium, and syncytia may form that do not plaque efficiently (Carpenter et al., 2009). Moreover, the connective tissue in skin makes it difficult to macerate into a single-cell suspension for plaque assay without destroying the infectivity of VZV. In this study we demonstrated how bioluminescence imaging could be successfully used to accurately measure VZV spread in cultured cells, in ex vivo skin organ culture, and in mice. This approach holds great promise for evaluating therapeutics for VZV and other viruses (Luker and Luker, 2008).

The ability to monitor VZV replication in the same mouse over time is a feature of bioluminescence imaging that not only reduces the number of animals required, but it also provides data on virus replication kinetics that were unobtainable with serial sacrifice and plaque assay (Moffat and Arvin, 1999). The rate of spread of VZV in skin implants was calculated as the Log_{10} (total flux/day) and was roughly linear from 2 to 10 dpi in untreated mice. It was interesting that treatment with PAA or roscovitine did not immediately halt the spread of VZV, although the growth rates decreased and the total flux was lower by the end of the treatment period. The continued momentum of virus spread during treatment is likely due to several factors: (1) luciferase gene expression is under control of the strong and constitutive SV40 IE promoter, (2) VZV-infected cells can transfer virus DNA to new cells where luciferase expression can proceed independently of VZV DNA synthesis, and (3) the mechanism of

action of the drugs may affect phases of VZV replication that occur later than the expression of luciferase. PAA acts upon the viral DNA polymerase and thereby prevents VZV late gene expression (Hay et al., 1977), which would not have an immediate effect on luciferase expression in the VZV-BAC-Luc strain. The antiviral mechanism of roscovitine is not fully understood for VZV, but we and others have reported that it prevents mRNA transcription from episomal viral genomes (Diwan et al., 2004; Schang et al., 2005; Taylor et al., 2004). This effect of roscovitine may prevent VZV replication, or roscovitine may inhibit CDK activity that is required for phosphorylation of the essential VZV proteins IE62 and IE63, which are known substrates of CDK1 (Habran et al., 2005; Leisenfelder et al., 2008). In either case, VZV-infected cells would have some ability to transfer pre-assembled virus to neighboring cells in the presence of inhibitory concentrations of roscovitine. If the virus spread by cell fusion, then luciferase would also be transferred and could maintain activity until the protein is degraded. Given the momentum of virus spread and luciferase expression during treatment, the efficacy of PAA and roscovitine in vivo were evaluated by their effects on virus growth rate and not on virus yield at a single time point. Different reporter gene promoters, such as those controlling VZV immediate early genes or true late genes, may affect the pattern of luciferase activity in infected cells and thus alter the apparent growth rates as measured by bioluminescence. Studies are currently underway to determine the suitability of various VZV-BAC strains for evaluating antiviral agents in this system.

For a virus such as VZV that causes skin lesions, cultivation of human skin ex vivo is an important intermediate model between cell culture and SCID-Hu mice for evaluating antiviral activity. SOC should provide a more representative model of natural VZV infection of skin than do skin cells in culture, and thus may provide a warning of problems with drug half-life or delivery in vivo. We found that all the compounds evaluated in this study had antiviral activity in HFFs, whereas acyclovir was less potent in SOC and aloisine A and purvalanol A were ineffective. In the case of purvalanol A, the results in SOC predicted the failure of the drug to inhibit VZV replication in vivo. Thus employing SOC may avert unnecessary tests in SCID-Hu mice, which are costly and limit the number of drug concentrations that can be compared in one cohort of animals. For compounds that are effective in SOC, the model can be especially useful for determining the drug EC_{50} in whole tissue and then using this information to estimate doses for mice. Lastly, daily bioluminescence imaging of infected skin explants gives rapid results and many replicates can be evaluated, thus increasing the statistical power of the tests.

The inability of aloisine A and purvalanol A to prevent VZV replication in SOC was unexpected, since both were effective in HFFs and purvalanol A had a particularly high SI. Several reasons can be posited, but a full explanation will require further studies. The two most likely possibilities are the route of delivery and the properties of the skin tissue. The full-thickness skin includes a layer of adipose tissue that could interfere with diffusion of the compounds from the medium (ex vivo) or the capillaries (in the mouse). However, there are no obvious features in the structure of aloisine A and purvalanol A that would explain why they did not reach the VZV-infected cells in skin while roscovitine did (Corbel et al., 2009; Meijer and Raymond, 2003). Precipitation of the compounds was not detected in the medium, alleviating concerns about solubility. Alternative routes of delivery may prove optimal for these compounds. For instance, problems with diffusion may have been averted by topical administration, either in a cream base or in DMSO solvent. In mice, 20 mg/kg/day purvalanol A was given by i.p. injection in a solvent of 50% DMSO and 25% ethanol in PBS, which was similar to another study that used the same dose and route to effectively treat tumors in C57B/6 mice (Goga et al., 2007). There were differences in the mouse strain (we used CB.17 background) and the diluent (Goga et al. used 100% DMSO). If purvalanol A had a very short half-life in mice, then it might not reach adequate concentration for antiviral efficacy. However, the $t_{1/2}$ for both roscovitine and purvalanol A in mice is approximately 1 h following i.v. injection (Raynaud et al., 2004). In this study, roscovitine in 50% DMSO was administered continuously via subcutaneous osmotic pump, which may have provided better pharmacokinetics for this class of drug. Perhaps if purvalanol A were administered subcutaneously it would attain an effective concentration in the skin implants. On the other hand, purvalanol A was not effective in skin ex vivo despite constant presence in the medium. Therefore, questions remain as to whether skin tissue presents special challenges in administering these compounds, or whether topical or continuous dosing is necessary. These issues are important for translational studies on antiviral drugs for VZV, since zoster is a cutaneous disease and drugs must be able to reach the infected cells in the dermis and epidermis.

To our knowledge, these are the first tests of roscovitine as an antiviral agent in vivo. It is of interest to study the antiviral properties of roscovitine as it is currently in phase 2b clinical trials for previously treated non-small cell lung cancer and nasopharyngeal cancer (CYC202 Seliciclib; Cyclacel Pharmaceuticals, Inc., Dundee, UK). There are potentially many other kinase inhibitors in the clinical trials pipeline that could be screened against viruses. Some have been identified, such as imatinib (targets receptor tyrosine protein kinases) that prevented poxvirus replication in mice and Kaposi's sarcoma herpesvirus tumors in HIV patients [reviewed by Schang (2006)]. Agents that target host cell functions may also have broad-spectrum activity if they block pathways required by a large family of viruses, i.e. the herpesviruses. For VZV, the combination of bioluminescence imaging and the SOC and SCID-Hu models will be essential for testing any new agents with promising antiviral activity. Current studies are directed toward optimizing the system for antiviral research.

Acknowledgements

We thank A. Arvin for the human antisera to VZV; C. Grose for the MeWo cell line; L. Meijer for CDK inhibitors; W. Wu for human β-globin clone; H. Zhu for VZV-BAC-Luc; S. Taylor and R. Morton for protocol advice and support. The Dean's Fund for Research Excellence supported RJG. Research support to JFM was from PHS (AI052168) and the Empire State Stem Cell Fund through New York State Department of Health Contract # C023059. Opinions expressed here are solely those of the author and do not necessarily reflect those of the Empire State Stem Cell Board, the New York State Department of Health, or the State of New York.

References

Alconada, A., Bauer, U., Hoflack, B., 1996. A tyrosine-based motif and a casein kinase II phosphorylation site regulate the intracellular trafficking of the varicella-zoster virus glycoprotein I, a protein localized in the trans-Golgi network. Embo J. 15, 6096–6110.

Babich, H., Sedletcaia, A., Kenigsberg, B., 2002. In vitro cytotoxicity of protocatechuic acid to cultured human cells from oral tissue: involvement in oxidative stress. Pharmacol. Toxicol. 91, 245–253.

Bresnahan, W.A., Boldogh, I., Chi, P., Thompson, E.A., Albrecht, T., 1997. Inhibition of cellular Cdk2 activity blocks human cytomegalovirus replication. Virology 231, 239–247.

Carpenter, J.E., Henderson, E.P., Grose, C., 2009. Enumeration of an extremely high particle-to-PFU ratio for Varicella-zoster virus. J. Virol. 83, 6917–6921.

Cohen, J.I., Sato, H., Srinivas, S., Lekstrom, K., 2001. Varicella-zoster virus (VZV) ORF65 virion protein is dispensable for replication in cell culture and is phosphorylated by casein kinase II, but not by the VZV protein kinases. Virology 280, 62–71.

Cohen, J.I., Straus, S.E., 2001. Varicella-zoster virus and its replication. In: Knipe, D.M., Howley, P.M. (Eds.), Fields Virology, vol.2, fourth ed. Lippincott-Raven, Philadelphia, pp. 2707–2730.

Corbel, C., Haddoub, R., Guiffant, D., Lozach, O., Gueyrard, D., Lemoine, J., Ratin, M., Meijer, L., Bach, S., Goekjian, P., 2009. Identification of potential cellular targets of aloisine A by affinity chromatography. Bioorg. Med. Chem. 17, 5572–5582.

De Clercq, E., 2004. Antiviral drugs in current clinical use. J. Clin. Virol. 30, 115–133.

Diwan, P., Lacasse, J.J., Schang, L.M., 2004. Roscovitine inhibits activation of promoters in herpes simplex virus type 1 genomes independently of promoter-specific factors. J. Virol. 78, 9352–9365.
Dothager, R.S., Flentie, K., Moss, B., Pan, M.H., Kesarwala, A., Piwnica-Worms, D., 2009. Advances in bioluminescence imaging of live animal models. Curr. Opin. Biotechnol. 20, 45–53.
Goga, A., Yang, D., Tward, A.D., Morgan, D.O., Bishop, J.M., 2007. Inhibition of CDK1 as a potential therapy for tumors over-expressing MYC. Nat. Med. 13, 820–827.
Habran, L., Bontems, S., Di Valentin, E., Sadzot-Delvaux, C., Piette, J., 2005. Varicella-zoster virus IE63 protein phosphorylation by roscovitine-sensitive cyclin-dependent kinases modulates its cellular localization and activity. J. Biol. Chem. 280, 29135–29143.
Hay, J., Brown, S.M., Jamieson, A.T., Rixon, F.J., Moss, H., Dargan, D.A., Subak-Sharpe, J.H., 1977. The effect of phosphonoacetic acid on herpes viruses. J. Antimicrob. Chemother. 3 (Suppl A), 63–70.
Holcomb, K., Weinberg, J.M., 2006. A novel vaccine (Zostavax) to prevent herpes zoster and postherpetic neuralgia. J. Drugs Dermatol. 5, 863–866.
Huang, E.S., Huang, C.H., Huong, S.M., Selgrade, M., 1976. Preferential inhibition of herpes-group viruses by phosphonoacetic acid: effect on virus DNA synthesis and virus-induced DNA polymerase activity. Yale J. Biol. Med. 49, 93–99.
Johnson, R.W., Wasner, G., Saddier, P., Baron, R., 2008. Herpes zoster and postherpetic neuralgia: optimizing management in the elderly patient. Drugs Aging 25, 991–1006.
Kabir, J., Lobo, M., Zachary, I., 2002. Staurosporine induces endothelial cell apoptosis via focal adhesion kinase dephosphorylation and focal adhesion disassembly independent of focal adhesion kinase proteolysis. Biochem. J. 367, 145–155.
Knockaert, M., Gray, N., Damiens, E., Chang, Y.T., Grellier, P., Grant, K., Fergusson, D., Mottram, J., Soete, M., Dubremetz, J.F., Le Roch, K., Doerig, C., Schultz, P., Meijer, L., 2000. Intracellular targets of cyclin-dependent kinase inhibitors: identification by affinity chromatography using immobilised inhibitors. Chem. Biol. 7, 411–422.
Knockaert, M., Lenormand, P., Gray, N., Schultz, P., Pouysségur, J., Meijer, L., 2002. p42/p44 MAPKs are intracellular targets of the CDK inhibitor purvalanol. Oncogene 21, 6413–6424.
Kudoh, A., Daikoku, T., Sugaya, Y., Isomura, H., Fujita, M., Kiyono, T., Nishiyama, Y., Tsurumi, T., 2004. Inhibition of S-phase cyclin-dependent kinase activity blocks expression of Epstein-Barr virus immediate-early and early genes, preventing viral lytic replication. J. Virol. 78, 104–115.
Leisenfelder, S.A., Moffat, J.F., 2006. Varicella-zoster virus infection of human foreskin fibroblast cells results in atypical cyclin expression and cyclin-dependent kinase activity. J. Virol. 80, 5577–5587.
Leisenfelder, S.A., Kinchington, P.R., Moffat, J.F., 2008. Cyclin-dependent kinase 1/cyclin B1 phosphorylates varicella-zoster virus IE62 and is incorporated into virions. J. Virol. 82, 12116–12125.
Luker, G.D., Bardill, J.P., Prior, J.L., Pica, C.M., Piwnica-Worms, D., Leib, D.A., 2002. Noninvasive bioluminescence imaging of herpes simplex virus type 1 infection and therapy in living mice. J. Virol. 76, 12149–12161.
Luker, K.E., Luker, G.D., 2008. Applications of bioluminescence imaging to antiviral research and therapy: multiple luciferase enzymes and quantitation. Antiviral Res. 78, 179–187.
Meggio, F., Shugar, D., Pinna, L.A., 1990. Ribofuranosyl-benzimidazole derivatives as inhibitors of casein kinase-2 and casein kinase-1. Eur. J. Biochem. 187, 89–94.
Meggio, F., Pinna, L.A., 2003. One-thousand-and-one substrates of protein kinase CK2? FASEB J. 17, 349–368.
Meijer, L., Raymond, E., 2003. Roscovitine and other purines as kinase inhibitors. From starfish oocytes to clinical trials. Acc. Chem. Res. 36, 417–425.
Mettey, Y., Gompel, M., Thomas, V., Garnier, M., Leost, M., Ceballos-Picot, I., Noble, M., Endicott, J., Vierfond, J.M., Meijer, L., 2003. Aloisines, a new family of CDK/GSK-3 inhibitors, SAR study, crystal structure in complex with CDK2, enzyme selectivity, and cellular effects. J. Med. Chem. 46, 222–236.
Moffat, J.F., Stein, M.D., Kaneshima, H., Arvin, A.M., 1995. Tropism of varicella-zoster virus for human CD4+ and CD8+ T lymphocytes and epidermal cells in SCID-hu mice. J. Virol. 69, 5236–5242.
Moffat, J.F., Zerboni, L., Kinchington, P.R., Grose, C., Kaneshima, H., Arvin, A.M., 1998. Attenuation of the vaccine Oka strain of varicella-zoster virus and role of glycoprotein C in alphaherpesvirus virulence demonstrated in the SCID-hu mouse. J. Virol. 72, 965–974.
Moffat, J.F., Arvin, A.M., 1999. Varicella-zoster virus infection of T cells and skin in the SCID-hu mouse model. In: Zak, O., Sande, M.A. (Eds.), Handbook of Animal Models of Infection. Academic Press, San Diego, pp. 973–980.
Moffat, J.F., McMichael, M.A., Leisenfelder, S.A., Taylor, S.L., 2004. Viral and cellular kinases are potential antiviral targets and have a central role in varicella zoster virus pathogenesis. Biochim. Biophys. Acta 1697, 225–231.
Mueller, N.H., Graf, L.L., Orlicky, D., Gilden, D., Cohrs, R.J., 2009. Phosphorylation of the nuclear form of varicella-zoster virus immediate-early protein 63 by casein kinase II at serine 186. J. Virol. 83, 12094–12100.
Nagaike, K., Mori, Y., Gomi, Y., Yoshii, H., Takahashi, M., Wagner, M., Koszinowski, U., Yamanishi, K., 2004. Cloning of the varicella-zoster virus genome as an infectious bacterial artificial chromosome in *Escherichia coli*. Vaccine 22, 4069–4074.
Niizuma, T., Zerboni, L., Sommer, M.H., Ito, H., Hinchliffe, S., Arvin, A.M., 2003. Construction of Varicella-zoster virus recombinants from parent oka cosmids and demonstration that ORF65 protein is dispensable for infection of human skin and T cells in the SCID-hu mouse model. J. Virol. 77, 6062–6065.
Oliver, S.L., Zerboni, L., Sommer, M., Rajamani, J., Arvin, A.M., 2008. Development of recombinant varicella-zoster viruses expressing luciferase fusion proteins for live in vivo imaging in human skin and dorsal root ganglia xenografts. J. Virol. Methods 154, 182–193.
Pedrali-Noy, G., Spadari, S., 1980. Mechanism of inhibition of herpes simplex virus and vaccinia virus DNA polymerases by aphidicolin, a highly specific inhibitor of DNA replication in eucaryotes. J. Virol. 36, 457–464.
Perry, C., Sastry, R., Nasrallah, I.M., Stover, P.J., 2005. Mimosine attenuates serine hydroxymethyltransferase transcription by chelating zinc. Implications for inhibition of DNA replication. J. Biol. Chem. 280, 396–400.
Pinna, L.A., Meggio, F., 1997. Protein kinase CK2 ("casein kinase-2") and its implication in cell division and proliferation. Prog. Cell Cycle Res. 3, 77–97.
Prather, R.S., Boquest, A.C., Day, B.N., 1999. Cell cycle analysis of cultured porcine mammary cells. Cloning 1, 17–24.
Raynaud, F.I., Fischer, P.M., Nutley, B.P., Goddard, P.M., Lane, D.P., Workman, P., 2004. Cassette dosing pharmacokinetics of a library of 2,6,9-trisubstituted purine cyclin-dependent kinase 2 inhibitors prepared by parallel synthesis. Mol. Cancer Ther. 3, 353–362.
Reardon, J.E., Spector, T., 1989. Herpes simplex virus type 1 DNA polymerase. Mechanism of inhibition by acyclovir triphosphate. J. Biol. Chem. 264, 7405–7411.
Renò, F., Tontini, A., Burattini, S., Papa, S., Falcieri, E., Tarzia, G., 1999. Mimosine induces apoptosis in the HL60 human tumor cell line. Apoptosis 4, 469–477.
Repetto, G., del Peso, A., Zurita, J.L., 2008. Neutral red uptake assay for the estimation of cell viability/cytotoxicity. Nat. Protoc. 3, 1125–1131.
Sampathkumar, P., Drage, L.A., Martin, D.P., 2009. Herpes zoster (shingles) and postherpetic neuralgia. Mayo Clin. Proc. 84, 274–280.
Sanchez, V., McElroy, A.K., Yen, J., Tamrakar, S., Clark, C.L., Schwartz, R.A., Spector, D.H., 2004. Cyclin-dependent kinase activity is required at early times for accurate processing and accumulation of the human cytomegalovirus UL122-123 and UL37 immediate-early transcripts and at later times for virus production. J. Virol. 78, 11219–11232.
Schang, L.M., Rosenberg, A., Schaffer, P.A., 2000. Roscovitine, a specific inhibitor of cellular cyclin-dependent kinases, inhibits herpes simplex virus DNA synthesis in the presence of viral early proteins. J. Virol. 74, 2107–2120.
Schang, L.M., Coccaro, E., Lacasse, J.J., 2005. Cdk inhibitory nucleoside analogs prevent transcription from viral genomes. Nucleosides Nucleotides Nucleic Acids 24, 829–837.
Schang, L.M., 2006. First demonstration of the effectiveness of inhibitors of cellular protein kinases in antiviral therapy. Expert Rev. Anti Infect. Ther. 4, 953–956.
Taylor, S.L., Kinchington, P.R., Brooks, A., Moffat, J.F., 2004. Roscovitine, a cyclin-dependent kinase inhibitor, prevents replication of varicella-zoster virus. J. Virol. 78, 2853–2862.
Taylor, S.L., Moffat, J.F., 2005. Replication of varicella-zoster virus in human skin organ culture. J. Virol. 79, 11501–11506.
Tischer, B.K., Kaufer, B.B., Sommer, M., Wussow, F., Arvin, A.M., Osterrieder, N., 2007. A self-excisable infectious bacterial artificial chromosome clone of varicella-zoster virus allows analysis of the essential tegument protein encoded by ORF9. J. Virol. 81, 13200–13208.
Vafai, A., Berger, M., 2001. Zoster in patients infected with HIV: a review. Am. J. Med. Sci. 321, 372–380.
Vázquez, M., LaRussa, P.S., Gershon, A.A., Niccolai, L.M., Muehlenbein, C.E., Steinberg, S.P., Shapiro, E.D., 2004. Effectiveness over time of varicella vaccine. JAMA 291, 851–855.
Verri, A., Maga, G., Spadari, S., Ponti, W., Strosselli, S., Bonizzi, L., Rocchi, M., Poli, G., Focher, F., 1994. Aphidicolin inhibits in vitro the activity of pseudorabies virus (PRV) DNA polymerase and in vivo the viral proliferation. In Vivo 8, 1041–1046.
Villerbu, N., Gaben, A.M., Redeuilh, G., Mester, J., 2002. Cellular effects of purvalanol A: a specific inhibitor of cyclin-dependent kinase activities. Int. J. Cancer 97, 761–769.
Wang, S., Fischer, P.M., 2008. Cyclin-dependent kinase 9: a key transcriptional regulator and potential drug target in oncology, virology and cardiology. Trends Pharmacol. Sci. 29, 302–313.
Wang, X., Rosol, M., Ge, S., Peterson, D., McNamara, G., Pollack, H., Kohn, D.B., Nelson, M.D., Crooks, G.M., 2003. Dynamic tracking of human hematopoietic stem cell engraftment using in vivo bioluminescence imaging. Blood 102, 3478–3482.
Yao, Z., Jackson, W., Grose, C., 1993. Identification of the phosphorylation sequence in the cytoplasmic tail of the varicella-zoster virus Fc receptor glycoprotein gpI. J. Virol. 67, 4464–4473.
Ye, M., Duus, K.M., Peng, J., Price, D.H., Grose, C., 1999. Varicella-zoster virus Fc receptor component gI is phosphorylated on its endodomain by a cyclin-dependent kinase. J. Virol. 73, 1320–1330.
Yoshii, H., Somboonthum, P., Takahashi, M., Yamanishi, K., Mori, Y., 2007. Cloning of full length genome of varicella-zoster virus vaccine strain into a bacterial artificial chromosome and reconstitution of infectious virus. Vaccine 25, 5006–5012.
Zapata, H.J., Nakatsugawa, M., Moffat, J.F., 2007. Varicella-zoster virus infection of human fibroblast cells activates the c-Jun N-terminal kinase pathway. J. Virol. 81, 977–990.
Zeuzem, S., 2008. Interferon-based therapy for chronic hepatitis C: current and future perspectives. Nat. Clin. Pract. Gastroenterol. Hepatol. 5, 610–622.
Zhang, Z., Rowe, J., Wang, W., Sommer, M., Arvin, A., Moffat, J., Zhu, H., 2007. Genetic analysis of varicella-zoster virus ORF0 to ORF4 by use of a novel luciferase bacterial artificial chromosome system. J. Virol. 81, 9024–9033.